Numerical Modelling of Mechanical Anisotropy during Low Temperature Nitriding of Stainless Steel

Kücükyildiz, Ömer C.; Sonne, Mads Rostgaard; Thorborg, Jesper; Winther, Grethe; Hattel, Jesper H.; Somers, Marcel A. J.

Publication date:
2018

Document Version
Peer reviewed version

Numerical Modelling of Mechanical Anisotropy during Low Temperature Nitriding of Stainless Steel

Ömer C. Kücükyildiz[1], Mads Rostgaard Sonne[1], Jesper Thorborg[2], Grethe Winther[1], Jesper H. Hattel[1], Marcel A.J. Somers[1]

[1]*Technical University of Denmark, Kgs. Lyngby, Denmark, omecak@mek.dtu.dk*

[2]*Magma GmbH, Aachen, Germany*

Abstract

A 3D Finite Element method (FEM) model for investigation of the anisotropic mechanical behaviour of austenitic stainless steel during nitriding is presented. The model considers the non-linear concentration dependent diffusion of nitrogen including trapping by chromium, the surface reaction, elastic and plastic anisotropy and influences on thermodynamics (solubility) and diffusion kinetics. Large differences in the nitrided case thickness have previously been attributed to the elastic and plastic anisotropy, which in turn affects the diffusion and solubility properties of nitrogen. The two mechanically distinctive grain orientations <001> and <111> are simulated and the stress, strain and concentration profiles are discussed and compared to experimental findings.

Keywords

Nitriding, diffusion, stresses, plasticity, anisotropy

1 Introduction

Low temperature nitriding of austenitic stainless steel leads to an advantageous combination of corrosion, wear and fatigue performance, which can be attributed to the development of a case of expanded austenite with a nitrogen composition-depth profile and an associated residual stress-depth profile [Somers, Christiansen 2015]. The stress arises from the volume expansion of the austenite by dissolving nitrogen, which is constrained by the untreated bulk. Previous work has demonstrated that a realistic prediction of the composition and stress profile from the nitriding parameters temperature, nitriding potential and time is not trivial [Jespersen et al. 2016, Kücükyildiz et al. 2017]. Such numerical modelling requires the consideration of the effects of mechanical (elastic) stress on the diffusive flux and the nitrogen solubility as well as the elastic and/or plastic accommodation of the volume expansion and the nitrogen concentration dependent thermal contraction during cooling after nitriding. Experimental observations for polycrystalline samples have shown that the case depth can vary from grain to grain. Arbitrarily, this has been attributed to elastic anisotropy or even hkl-dependent diffusion coefficients [Martinavičius et al. 2009], which in principle is in conflict with the isotropy of diffusion in a cubic lattice. Earlier the hkl dependence of the case depth after plasma nitriding of a nickel base alloy was shown to scale with the anisotropy factor [He et al. 2003]. Most likely also the plastic anisotropy plays a role in the affecting the case depth. At least plastic deformation in fcc affects the strong elastic anisotropy in deformed expanded austenite leading to anomalous peak shifts of particularly the 200 reflection in X-ray diffractograms [Brink et al. 2017].

So far, modelling attempts have only considered isotropic elastic and plastic behaviour of austenite. As is well-known austenite is strongly elastically anisotropic as reflected by a variation of the Young's modulus by a factor three: the <111> direction is approximately three times as stiff as the <001> direction. Obviously also plastic deformation is anisotropic, as it depends on

the orientation of the (active) slip planes with respect to the stress state. During plastic deformation of an fcc grain, a rotation is induced [Bishop and Hill], which changes the effective critical resolved shear stress.

In the present work, the effect of elastic and plastic anisotropy on the case depth of expanded austenite during low temperature gas nitriding of stainless steel is investigated by incorporating the hkl dependence of the elastic and plastic properties. To this end a coupled temperature-displacement 3D Finite Element Model (FEM) was adopted and modified for solving diffusion problems rather than heat conduction.

The anisotropic expansion of the expanded austenite lattice causes a stress state that depends on the orientation. By aligning the orientation of the surface normal along the <001> and <111> directions of the fcc lattice, two extreme cases of stress distributions and the consequent nitrogen depth-profiles are simulated. In this work, it is assumed that no lattice rotation takes place during plastic deformation. The results are compared with experimental findings.

2 Methods

The developed 3D model is based on the Finite Element Method using the commercial software Abaqus in combination with user-defined sub-routines. The simulation combines concentration-dependent diffusion, trapping of nitrogen by chromium, lattice expansion, anisotropic elastic and plastic accommodation (including work hardening) of the lattice expansion and the kinetics of the transfer of nitrogen from gas to solid, i.e. the surface reaction.

The concentration profile is calculated based on a modified Fick's 2nd law, with a non-linear diffusion coefficient and a composition-induced stress gradient, which induces an additional driving force for diffusion. The modified Fick's 2nd law was derived in [Jespersen, Hattel, Somers 2016], and in the current work is used without the temperature gradient effect due to the isothermal problem:

$$\frac{\partial c_N}{\partial t} = \frac{\partial D_N}{\partial c_N} \cdot \left(\frac{\partial c_N}{\partial z}\right)^2 + D_N \cdot \frac{\partial^2 c_N}{\partial z^2} - \frac{\partial}{\partial z}\left(\frac{D_N}{\frac{\partial K_N}{\partial c_N}} \cdot \frac{K_N}{T}\right) \cdot \frac{V_N}{R} \cdot \frac{\partial \sigma_H}{\partial z} - D_N \cdot \frac{K_N}{\frac{\partial K_N}{\partial c_N}} \cdot \frac{V_N}{R \cdot T} \cdot \frac{\partial^2 \sigma_H}{\partial z^2} \qquad (1)$$

where c_N is the nitrogen concentration, D_N the nitrogen dependent diffusion coefficient, K_N the nitriding potential, R the gas constant, V_N the partial molar volume of nitrogen and T the temperature. The solubility of nitrogen in the surface is an inverse function of the hydrostatic stress level in the surface of the fcc lattice [Christiansen, Somers 2006]:

$$\ln(a_N^{\sigma}) = \ln(a_N^{\sigma=0}) - \frac{V_N \sigma_H}{RT} \qquad (2)$$

where α is the nitrogen activity and σ_H the hydrostatic stress component in the surface.

The coupled diffusion-displacement model to be formulated is a straightforward application of the coupled-temperature-displacement analysis in Abaqus, taking the heat capacity (c_p) and density value (ρ) to unity and replacing the thermal conductivity (k) by the diffusion coefficient (D). The stress gradients, which were not readily available, and their effect on diffusion, were estimated using the shape functions of the second order elements following the method described in [Barrera et al. 2016].

Single crystals with the <001> and <111> directions perpendicular to the surface, i.e. parallel to the direction of the nitrogen diffusion, were simulated by specifying the local material orientation with respect to the global orientation. One of the transverse directions $[1\bar{1}0]$ was chosen such that the two orientations coincide in order to make a direct comparison of the results.

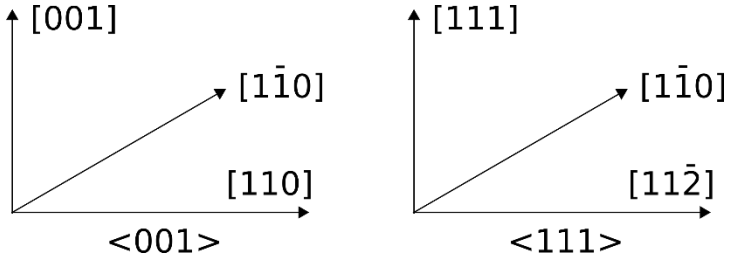

Figure 1: the <001> and <111> crystal orientations and their directions

Elastic anisotropy was implemented as an orthotropic type with the elastic stiffness coefficients: $C_{11} = 215.9 * 10^9$, $C_{12} = 144.6 * 10^9$ and $C_{44} = 128.9 * 10^9$. The coefficients are related to the elastic modulus by:

$$\frac{1}{E_{hkl}} = C_{11} - (2C_{11} - C_{12} - C_{44})A_{hkl} \tag{3}$$

with the anisotropy parameter

$$A_{hkl} = \frac{(h^2k^2+h^2l^2+k^2l^2)}{(h^2+k^2+l^2)^2} \tag{4}$$

The Young's moduli for three crystallographic directions <hkl> are given in Table 1. Plastic anisotropy was assumed to scale with the Taylor factor, M, for the respective <hkl>. The critically resolved shear stress was obtained from hardness measurements on polycrystalline expanded austenite using the (averaged) Taylor factor $M = 3.02$.

Orientation	**Taylor factor (M)**	**Yield stress [MPa] (c_N > [mol/m^3])**	**E-modulus [GPa]**
<001>	2.45	3034 (19300)	100
<011>	3.67	4552 (14550)	202
<111>	3.67	4552 (9680)	308
polycrystal	3.02	3746 (14796)	180

Table 1: The anisotropic elastic and plastic mechanical properties for the two investigated single crystal orientations <001> and <111>. The properties of the <011> single crystal orientation and polycrystal are shown for comparison.

Hardness tests on polycrystalline steel with a range of nitrogen contents revealed a strongly concentration dependent yield strength up to a certain nitrogen content [Bottoli et al. 2016, Jespersen et al. 2016] . The slope in the strengthening part of the stress-strain relation (cf. Fig. 1) commensurate with the elastic stiffness of the austenitic stainless steel. Solid solution strengthening by nitrogen atoms proceeds until a yield strength plateau is reached, beyond which no further increase is observed (corresponding to a hardness plateau in expanded austenite zones). Both the elastic stiffness and the effective yield strength depend on the orientation of a grain (and thus its slip planes) with respect to the loading direction. The data from Table 1 thus give the yield strength as a function of concentration and orientation as shown in Figure 2.

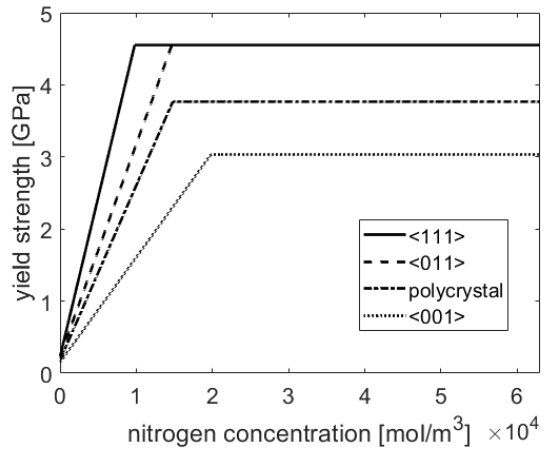

Figure 2: Concentration and orientation dependent yield strength without work hardening effect

3 Results

The nitriding parameters used in the simulations were identical to those used for nitriding single crystal 316 stainless steel samples in [Somers, Christiansen 2015]; the treatment time was set to t = 14 h at temperature T = 440 °C and a nitriding potential (or, equivalently, a nitrogen activity) $K_N = \infty$.

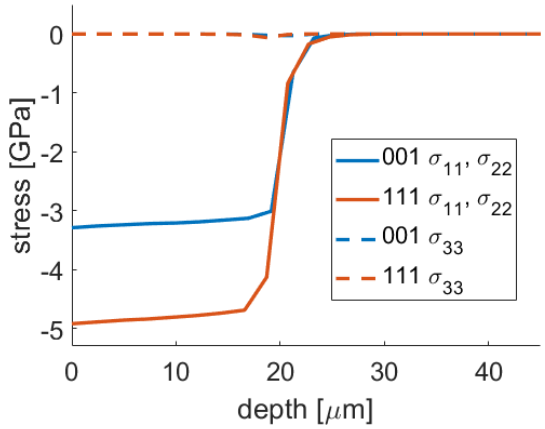

Figure 3: The (elastic) stress profiles along the diffusion direction σ_{33} and within the plane of the crystal $(\sigma_{11}, \sigma_{22})$ for the two orientations <001> and <111>

The elastic and plastic anisotropy are observed as the slope of the elastic region and the stress-level at the surface region, respectively. The stress level with the addition of that of work hardening is $\sigma_{11} = \sigma_{22} = -3.29$ GPa for <001> and $\sigma_{11} = \sigma_{22} = -4.91$ GPa for <111>, following the yield flow values in Figure 2. The surface normal stresses are zero as expected. The stress distributions give hydrostatic stress levels of $\sigma_H = -2$ and -3 GPa, respectively.

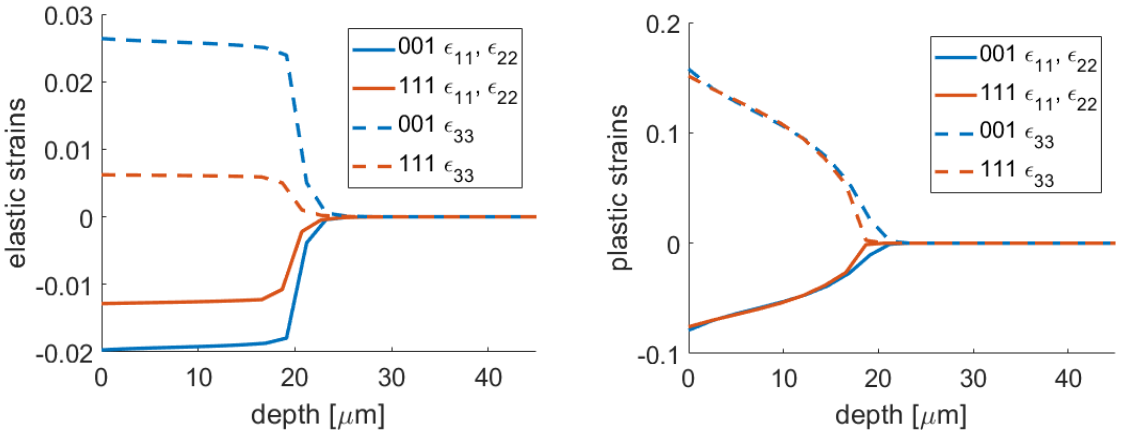

Figure 4: (a) the elastic and (b) plastic strain profiles for the two orientations <001> and <111>

The elastic strains vary according to the crystal orientation and a smallest elastic strain is observed for the stiffer <111> direction. The ratio between the in-plane strain components and the strain normal to surface are different for the two orientations. For <111> the in-plane strain is largest, while for <001> the elastic strain is largest along the surface normal.

The plastic strains are nearly identical, with exception of the depth region where mainly elastic accommodation occurs. This appears in contrast with the expectation that the stiffer <111> direction has the largest plastic deformation. The higher nitrogen concentration in <001> (Figure 5) explains why the plastic strains in <001> and <111> do overlap (Figure 4). A maximum plastic deformation of 16 % is observed, which is consistent with earlier estimates.

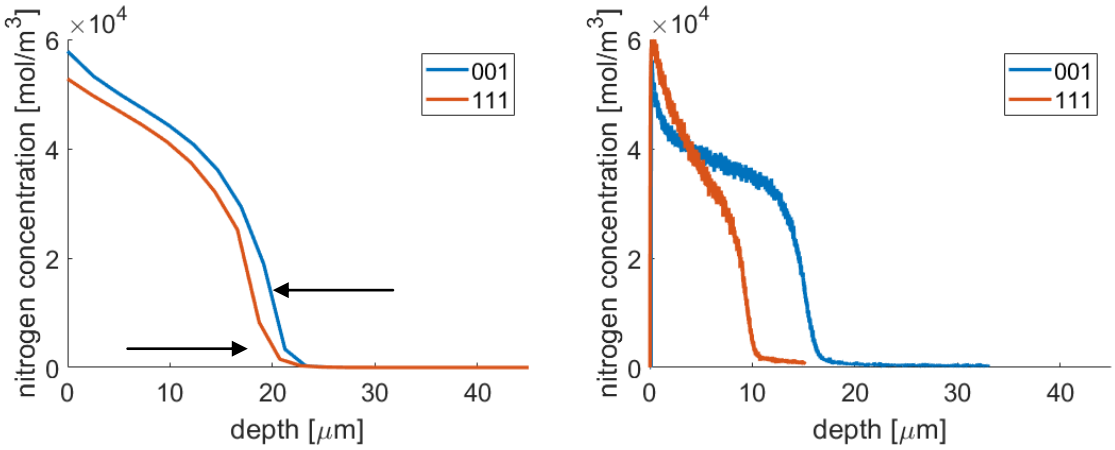

Figure 5: (a) the concentration profiles for the two orientations <001> and <111> and (b) the experimental concentration profiles determined with GD-OES for single crystals with the same orientations. The arrows indicate the concentration at which the orientation reaches maximum yield strength.

Stress-induced diffusion caused by the hydrostatic stress gradient in combination with the higher solubility in the <001> grain has the net effect that it experiences a case deeper by about 14 % as compared to the <111> grain. The nitrogen concentration (and corresponding depth) where the yield stress is reached, is marked by the arrows in Figure 5a. The experimental profiles are shown in Figure 5b, which shows difference in treatment depth of 50 % as well as different slopes in the plastic region.

4 Discussion

Recognizing that the <111> and <001> orientations are not sensitive for lattice rotation, the orientation dependent yield stress was assumed to follow a Taylor crystal plasticity theory.

The experimental case depth was measured to differ by 50 % between the two orientations. The numerical simulations show only 14 % difference, which is largely due to different surface concentrations. The difference in the surface stresses between <111> and <001> crystals leads to different nitrogen solubilities (cf. Eq. 2). [Wu et al. 2014] found a difference in case depth of 70 % between <001> and <111> orientations, which was ascribed to an experimentally determined difference in the surface concentration of grains. This correlates qualitatively with our modelling attempts. In our modelling attempts the difference between <001> and <111> may be underestimated, because the introduction of plastic deformation in austenitic stainless steel (and presumably also in expanded austenite) has a strong influence on the elastic behaviour of particularly the <001> oriented grains. This follows from the graph in Figure 6 showing the lattice strain as determined with neutron diffraction of various grain orientations in a polycrystalline material on the applied tensile stress (data from [Clausen, Lorentzen, Leffers 1998]; graph from [Brink, et al. 2017]).

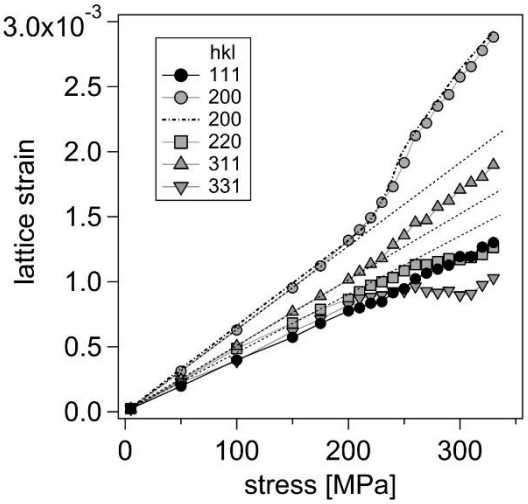

Figure 6: Experimental lattice strains for selected *hkl* as measured with neutron diffraction in the direction parallel to the uniaxial tensile stress applied onto austenitic stainless steel. For comparison the predicted lattice strain for 200 is included and represented by the dash-dot line (all experimental data and simulations from [Clausen, Lorentzen, Leffers 1998]). The thin dashed straight lines extrapolate the elastic regime for 200, 220 and 311 reflections to emphasize the non-linearities introduced by plastic deformation.

The net diffusion as a consequence of the stress gradient effect can be seen as the area under the solid solution strengthening part of the yield curves, which would give an approximately 33 % difference in the stress gradient enhanced diffusion effect. In this light, the gradient effect was expected to result in a greater difference in treatment depth between the two orientations. Similarly, the limiting effect of the hydrostatic stress level on the diffusion coefficient in the fcc lattice is not considered. The difference in magnitude of the calculated hydrostatic stresses is 50 % higher in the <111> orientation, which may explain the experimentally observed smaller case depth.

For identical concentration profiles, a greater plastic deformation would be expected for the stiffer <111> orientation, since it reaches the yield strength at a lower nitrogen content by a factor 2. Conversely, a greater elastic deformation is observed for the <001> direction.

5 Conclusion

A 3D Finite Element anisotropic model was introduced to investigate the influence of grain orientation on the mechanical properties and consequently the nitrogen distribution during low temperature nitriding of stainless steel. Qualitatively, the simulated concentration profiles were in agreement with experimental observations. However, the expected highly orientation

dependent concentration profiles were not reproduced. The proposed explanations for the discrepancy were the strong influence of plastic deformation on the elastic constants, especially in the case of the <001> orientation and the absence of the pressure effect on the diffusion coefficient.

The initial attempt at numerically modelling the mechanically anisotropic effect and thereby the orientation dependent concentration profiles gives a good insight in the challenges and complexities of the underlying mechanisms.

Acknowledgement

Part of this work has been supported by the Strategic Research Center "REWIND – Knowledge based engineering for improved reliability of critical wind turbine components," Danish Research Council for Strategic Research, grant no. 10-093966.

References

Barrera, O., E. Tarleton, H. W. Tang, and A. C. F. Cocks. 2016. "Modelling the Coupling between Hydrogen Diffusion and the Mechanical Behaviour of Metals." *Computational Materials Science* 122:219–28. Retrieved (http://dx.doi.org/10.1016/j.commatsci.2016.05.030).

Brink, Bastian K. et al. 2017. "On the Elusive Crystal Structure of Expanded Austenite." *Scripta Materialia* 131:59–62.

Christiansen, Thomas and Marcel a. J. Somers. 2006. "Controlled Dissolution of Colossal Quantities of Nitrogen in Stainless Steel." *Metallurgical and Materials Transactions A* 37(3):675–82.

Clausen, B., T. Lorentzen, and T. Leffers. 1998. "Self-Consistent Modelling of the Plastic Deformation of F.c.c. Polycrystals and Its Implications for Diffraction Measurements of Internal Stresses." *Acta Materialia* 46(9):3087–3098.

He, H., T. Czerwiec, C. Dong, and H. Michel. 2003. "Effect of Grain Orientation on the Nitriding Rate of a Nickel Base Alloy Studied by Electron Backscatter Diffraction." *Surface and Coatings Technology* 163–164:331–38.

Jespersen, Freja N., Jesper H. Hattel, and Marcel A. J. Somers. 2016. "Modelling the Evolution of Composition-and Stress-Depth Profiles in Austenitic Stainless Steels during Low-Temperature Nitriding." *Modelling and Simulation in Materials Science and Engineering* 24(2):25003. Retrieved (http://dx.doi.org/10.1088/0965-0393/24/2/025003).

Kücükyildiz, Ömer C., Mads Rostgaard Sonne, Jesper Thorborg, Jesper H. Hattel, and Marcel A. J. Somers. 2017. "Integrated Computational Modelling of Thermochemical Surface Engineering of Stainless Steel." in *Proceedings of the 24th Ifhtse Congress*. Retrieved March 5, 2018 (http://findit.dtu.dk/en/catalog/2372008924).

Martinavičius, A. et al. 2009. "Anisotropic Ion-Enhanced Diffusion during Ion Nitriding of Single Crystalline Austenitic Stainless Steel." *Journal of Applied Physics* 105(9).

Mittemeijer, E. J. and Marcel A. J. Somers. 2015. *Thermochemical Surface Engineering of Steels : Improving Materials Performance*. Woodhead Publishing. Retrieved September 18, 2017 (http://findit.dtu.dk/en/catalog/2201776628).

Somers, M. A. J. and T. L. Christiansen. 2015. *Hardening of Stainless Steel*.

Wu, D. et al. 2014. "ScienceDirect Orientation Dependence of Nitrogen Supersaturation in Austenitic Stainless Steel during Low-Temperature Gas-Phase Nitriding." 79:339–50.